CHEMICAL ENGINEERING TRANSACTIONS
VOL. 56, 2017
A publication of AIDIC
The Italian Association of Chemical Engineering
Online at www.aidic.it/cet
Guest Editors: Jiří Jaromír Klemeš, Peng Yen Liew, Wai Shin Ho, Jeng Shiun Lim
Copyright © 2017, AIDIC Servizi S.r.l.,
ISBN 978-88-95608-47-1; **ISSN** 2283-9216
DOI: 10.3303/CET1756054

Photocatalytic Reverse Water Gas Shift CO_2 Reduction to CO over Montmorillonite Supported TiO_2 Nanocomposite

Muhammad Tahir*, Beenish Tahir, Nor Aishah Saidina Amin

Chemical Reaction Engineering Group (CREG), Department of Chemical Engineering, Faculty of Chemical and Energy Engineering, Universiti Teknologi Malaysia (UTM), 81310 UTM Johor Bahru, Johor, Malaysia.
mtahir@cheme.utm.my

Photocatalytic CO_2 reduction by H_2 to CO via reverse water gas shift (RWGS) reaction over Montmorillonite (MMT) dispersed TiO_2 nanoparticles has been investigated. MMT-clay supported TiO_2 nanocomposites were prepared by a controlled and direct sol-gel method and were dip-coated over the monolith channels. The samples were characterized by XRD, FTIR, SEM, N_2-adsorption-desorption and UV–visible spectroscopy. The performance of nanomaterials was tested in a continuous operation of monolith photoreactor for dynamic CO and hydrocarbons production under UV-light irradiation. The photoactivity of MMT/TiO_2 nanocomposites loaded over the monolith channels was expressively increased for CO_2 reduction to CO as the main product. The maximum yield of CO over 10 wt. % MMT-loaded TiO_2 catalyst obtained was 25.95 µmole g-catal.$^{-1}$ h^{-1} at selectivity 98 %, considerably higher than the amount produced over the pure TiO_2 (8.52 µmole g-catal.$^{-1}$ h^{-1}). The other products detected with adequate amounts were CH_4 and C_2H_6. This significant enhancement in CO evolution was evidently due to efficient light distribution with larger illuminated active surface area inside monolith micro-channels and hindered charges recombination rate over MMT dispersed TiO_2. The reaction mechanism to understand the route of CO_2 reduction by H_2 via RWGS reaction is also proposed. This development has confirmed higher performance of green MMT/TiO_2 photo-catalyst for continuous CO_2 photo-reduction to cleaner fuels.

1. Introduction

Carbon dioxide (CO_2) is widely available as an inexpensive feedstock, but it is the primary cause of global warming. The excessive burning of fossil fuels and human activities such as deforestation has increased the level of CO_2 in the atmosphere. On the other hand, CO_2 is a stable molecule and its conversion to chemicals and fuels using thermal catalytic process is an energy-consuming process (Yang et al., 2016). The photocatalytic CO_2 conversion to fuels by the use of light irradiation, more preferably sunlight, provides pathways towards economical and sustainable process (Tahir et al., 2015b). However, most of the work in the field of photocatalytic CO_2 reduction has been related to using water as a reducing agent. However, H_2O is hardly reducible and CO_2 conversion by H_2O yielded lower amounts of products with lesser selectivity (Olivo et al., 2015). Recently, CO_2 conversion to fuels by hydrogen as a reducing agent through photocatalytic reverse water gas shift (RWGS) reaction has been reported as the most attractive method (Tahir et al., 2015a).

Among the various semiconductor materials, titanium dioxide (TiO_2) has attracted many researchers in recent years due to its numerous advantages such as relatively low price, available in excess, photo-stable, non-toxic and has high oxidative potentials (Paulino et al., 2016). However, TiO_2 photocatalytic efficiency is lower because of fast recombination of photo-generated electron holes pairs. One of the potentials to enhance TiO_2 photocatalytic activity is by its dispersion into the clay micro-sheets. Using nanoclay as a support in which TiO_2 can be distributed on the surface of a suitable matrix, clay-TiO_2 hetero-junction is formed (Kameshima et al., 2009).

The most widely used clay minerals for photocatalytic applications is montmorillonite (MMT). MMT is multilayered nano-clay in which one octahedral sheet is sandwiched between two silica tetrahedral sheets

Please cite this article as: Tahir M., Tahir B., Amin N.A.S., 2017, Photocatalytic reverse water gas shift co2 reduction to co over montmorillonite supported tio2 nanocomposite, Chemical Engineering Transactions, 56, 319-324 DOI:10.3303/CET1756054

(Chen et al., 2012). This characteristic of MMT makes it suitable for high sorption capacity in addition of charge trapping ability. By dispersing TiO_2 over MMT layers clay-TiO_2 hetero-junction is produced, resulting in the enhanced TiO_2 photocatalytic activity. Previously, we have investigated MMT loaded TiO_2 nanocomposite for photocatalytic CO_2 reduction with H_2O and observed significant amount of CH_4 production (Tahir et al., 2013). It is obvious from the literature that MMT is the most widely studied clay for the growth of TiO_2 nanoparticles. However, the enhanced photocatalytic reduction ability of MMT/TiO_2 composite has so far been demonstrated for CO_2 reduction by water as a reducing agent in a batch mode of operation. In this context, further research involving photocatalytic reverse water gas shift reaction over MMT supported TiO_2 for gas phase systems in a continuous monolith photoreactor to produce renewable fuels is warranted.
The objective of the present work is to use MMT-nanoclay to modify TiO_2 structure for photocatalytic CO_2 reduction by H_2 reducing agent via RWGS reaction. MMT/TiO_2 nano-composite was loaded over the monolith microchannels and photocatalytic activity was investigated in continuous operation of photoreactor. The photocatalysts were synthesized by sol-gel-dip coating method and were characterized by XRD, field emission scanning electron microscopy (FE-SEM), FTIR, N_2 adsorption-desorption isotherms, BJH pore size distribution, and UV-Vis spectroscopy. In addition, the photocatalytic reaction mechanism for CO_2 reduction to CO were analysed based on the experimental results.

2. Experimental

2.1 Catalyst preparation

The MMT-loaded TiO_2 nanocomposites were synthesized through a direct and single step sol-gel method according to our previous work (Tahir et al., 2016b). Typically, 10 mL titanium solution dispersed in 30 mL isopropanol was taken into flask for the hydrolysis process. Next, the solution was hydrolyzed by adding 7 mL acetic acid (1M) diluted in 10 mL isopropanol under vigorous stirring. The mixture was stirred for 24 h to get clear titanium sol. Subsequently, MMT dispersed in isopropanol was added into titanium sol. The process of gelation was continued by stirring the mixture for another 6h until the thick sol was obtained. The sol obtained was transferred into a glass container and was coated over the monolith channels. The coated monoliths were dried at 80 ^oC for 12 h before calcined at 500 ^oC for 5 h.

2.2 Characterization

The crystalline phase was investigated using powder X-ray diffraction (XRD; Bruker D8 advance diffractometer, 40 kV and 40 mA) with Cu- Kα radiation (λ= 1.54 A^o). The infrared spectra was measured at room temperature in the range of 4000 to 400 cm^{-1} with Spectrum 2000 Explorer Fourier Transformed Infrared (FT-IR) Spectrometer. The scanning electron microscopy (SEM) was carried out with JEOL JSM6390 LV SEM instrument. The specific surface area and pore diameters were measured by a Thermo scientific Surfer analyzer with nitrogen sorption at 77 K, degassing at 250 °C for 4 h and analyzed by the Brunauer Emmett Teller (BET) method. UV-Vis diffuse reflectance absorbance spectra were determined using UV-vis spectrophotometer (Agilent, Cary 100) equipped with an integrated sphere.

2.3 Photoactivity test

The reactor consists of stainless steel cylindrical vessel with a length of 5.5 cm and total volume of 150 cm^3 (Tahir et al., 2016a). The catalyst coated monoliths were introduced inside the cylindrical stainless steel chamber, equipped with a quartz window for passing light irradiations using 200W Hg lamp. Prior to feeding, the reactor chamber was purged using purified helium (He) flow, then a mixture of gases (CO_2, H_2 and He) was constantly streamed through the reactor for 1 h to saturate the catalyst. The products were analyzed using an on-line gas chromatograph (GC-Agilent Technologies 6890 N, USA) equipped with thermal conductivity detector (TCD) and flame ionized detector (FID). Furthermore, FID detector was connected with a HP-PLOT Q capillary column and TCD detector was connected to UCW982, DC-200, Porapak Q and Mol Sieve 13X columns.

3. Results and discussion

3.1 Catalyst characterization

Figure 1 (a) shows the XRD patterns of TiO_2, MMT and MMT/TiO_2 nano-composites. The peaks of TiO_2 NPs calcined at 500 ^oC revealed a pure anatase and crystalline phase. The XRD pattern of MMT presents a broad basal reflection of (0 0 1) at $2\theta = 3.70^o$, evidently due to the orientation of platy-shaped particles and stacking disorder of MMT layers. In the case of TiO_2 dispersed over the MMT layers, TiO_2 persisted its original reflection with no additional peaked appeared, however, TiO_2 peaks in MMT/TiO_2 sample were broader and

weaker, while prominent MMT peak (001) due to the layered clay has disappeared. This revealed that the layered structure of the MMT has disordered with uniform dispersion of TiO_2 NPs. This resulted in controlled crystal growth of TiO_2 NPs with the meso-porous structure (Tahir et al., 2015c).
Figure 1 (b) shows Infrared spectra of TiO_2, MMT and MMT/TiO_2 samples. The stretching bend at 1615 cm^1 in the spectrum of the pure TiO_2 NPs, showed chemisorbed H_2O in TiO_2 is negligible. The IR spectrum of MMT presents broadband at around 3,630 cm^{-2} attributed to Al_2OH group of octahedral layer, while the bands at around 3,460 cm^{-1} and 1,630 cm^{-1} can be allocated to -OH and stretching and bending vibration of water molecules. The peak at 1,047 cm^{-1} corresponds to a symmetric vibration of SiO_2 tetrahedra while several peaks between 1,000 and 500 cm^{-1} can be attributed to Al-IV tetrahedra. The peaks between 500 and 400 cm^{-1} were assigned to bending vibration of Si-O. On the other hand, MMT/TiO_2 sample shows similar patterns of peaks as like that TiO_2 and MMT samples with some new peaks. The stretching band at about 1,088 cm^{-1} and very week stretching at 450 to 550 cm^{-1} were observed due to the asymmetric stretching vibration of SiO_2 tetrahedra. A new peak at 930 cm^{-1} corresponds to Si-O-Ti bond which also discloses that TiO_2 combines with MMT by the formation of Si-O-Ti chemical bond (Tahir et al., 2013).

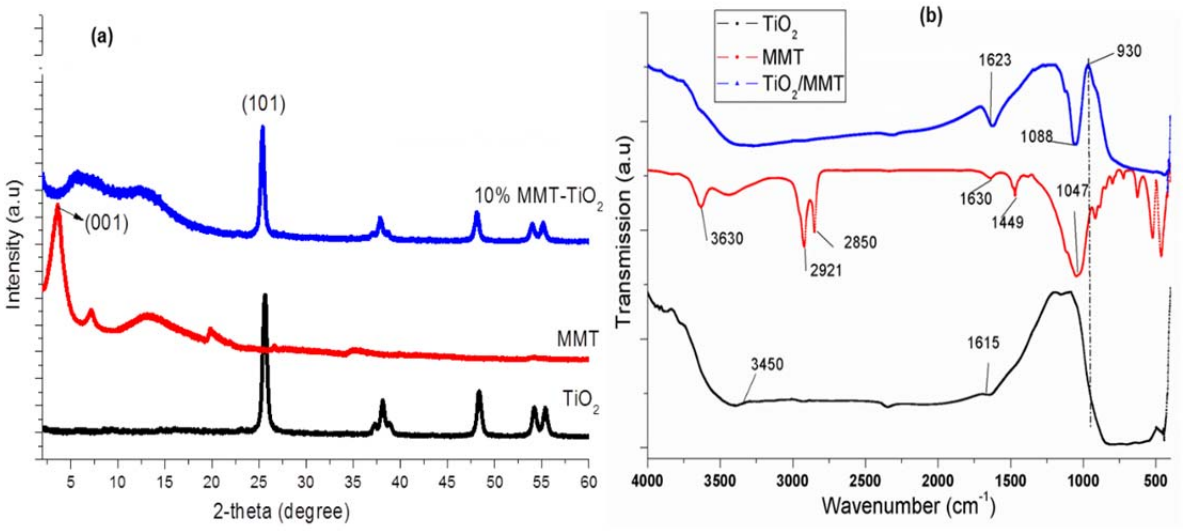

Figure 1: (a) X-ray diffraction patterns of TiO_2, MMT and MMT/TiO_2 catalysts; (b) FTIR spectra of the corresponding samples.

The structure and morphology of TiO_2, MMT and MMT/TiO_2 samples is presented in Figure 2. The MMT images in Figure 2(a) and (b) showed uniform and almost smooth MMT sheets with layered structures. The uniform, spherical in shape and mesoporous TiO_2 nano-particles could be seen in Figure 2(c). Figure 2(d) illustrates SEM images of TiO_2 dispersion over the MMT layers. Evidently, MMT layers are completely destroyed and TiO_2 NPs are well distributed over the MMT surface, confirming efficient intercalation process, thus producing delaminated MMT/TiO_2 nanocomposite.
The N_2-adsorption-desorption isotherms of the pure TiO_2 and MMT/TiO_2 samples were conducted to measure the BET surface area, pore size and pore volume of all the samples as summarized in Table 1. BET specific surface area (S_{BET}) of the pure TiO_2 NPs was 43, increased to 52 m^2/g, when 10 wt.% MMT was dispersed with TiO_2 NPs. This increased in BET surface area was evidently due to efficient dispersion of TiO_2 over MMT layered structure. In the case of pore diameter, pure TiO_2 pore diameter was 11 nm, reduced to 9 nm in MMT/TiO_2, obviously due to the controlled crystal growth over MMT layers. Similar observations were obtained in BJH adsorption pore volumes. The UV–vis diffuse reflectance absorbance spectra of TiO_2 and MMT/TiO_2 samples were obtained to measure the band gap energy. The band gap energy was calculated according to plot of $(\alpha h\nu)^2$ vs. photon energy. The band gap energy of 3.11 and 3.8 eV was obtained for TiO_2 and MMT/TiO_2 samples, respectively. It is obvious that there is a gradual decrease in the band gap energy in MMT-loaded TiO_2 samples compared to pure TiO_2 NPs.

Table 1: Summary of physiochemical analysis of TiO_2 and MMT dispersed TiO_2 samples

Samples	BET surface area (m^2/g)	BJH surface area (m^2/g)	BJH pore volume (cm^3/g)	Pore diameter (nm)	Band gap energy (eV)
TiO_2	43	52	0.135	11	3.11
10% MMT/TiO_2	52	48	0.103	9	3.8

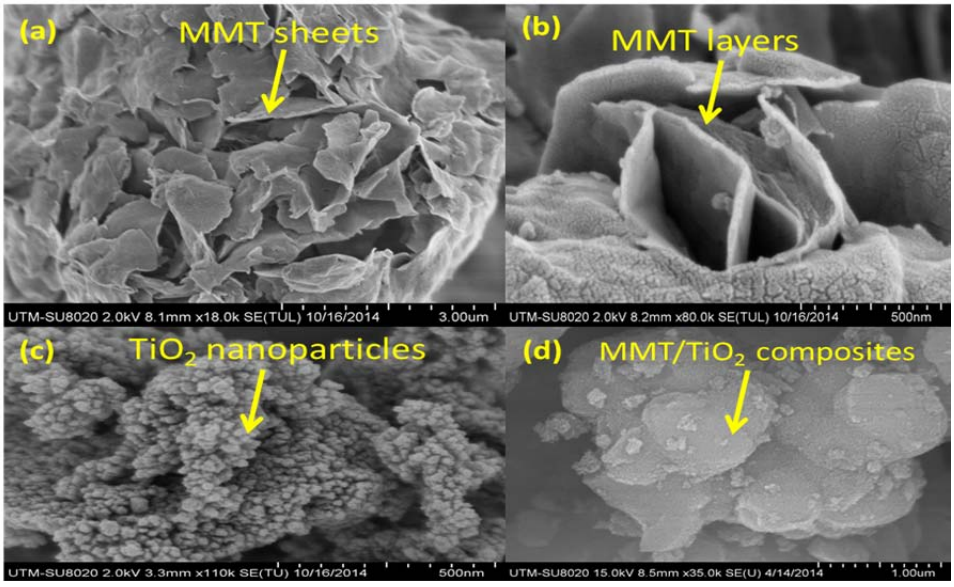

Figure 2: SEM images of TiO_2 and TiO_2/MMTs samples: (a-b) SEM images of MMT layers; (c) SEM image of TiO_2 nanoparticles, (d) SEM image of TiO_2/MMT sample.

3.2 Photocatalytic CO_2 reduction with H_2

Firstly, control experiments for photocatalytic RWGS reaction were conducted in the presence of photocatalysts. Using all types of catalysts, carbon containing compounds were not detected in the reaction system without reactants or light irradiations. Thus, any carbon containing compounds produced were derived from CO_2 photo-reduction with CO found to be a major CO_2 photo-reduction product in all the experiments. The effects of MMT onto TiO_2 performance for CO_2 photo-reduction with H_2 to CO and CH_4 is presented in Figure 3(a). CO was detected as the main product over all types of photo-catalysts which has confirmed favourable RWGS reaction using monolith as the photoreactor and hydrogen as a reducing agent. Pure TiO_2 has low photoactivity for CO production, which gradually increased in MMT supported TiO_2 samples. This was evidently due to efficient charge transfer, higher surface area and efficient CO_2 adsorption in MMT/TiO_2 samples. Loading MMT into TiO_2 significantly improved CO_2 photoreduction with optimum MMT-loading of 10 wt.%. 10 wt.% MMT-loaded TiO_2 sample was the most active over which continuous production of CO was the highest. However, with more MMT loading (e.g., 15 wt.%) into TiO_2, photoactivity was gradually reduced. This was certainly reduced in photo-catalyst (TiO_2) active sites and perhaps due to shading effect inside the monolith micro-channels by excessive MMT-loading.

Figure 3 (b) shows the effect of irradiation time on continuous production of CO during RWGS reaction using various MMT-loading TiO_2 samples at CO_2/H_2 ratio 1.0, 100^oC and feed flow rate 20 mL/min. Initially, much higher dynamic CO evolution was detected in all the samples which were gradually reduced after 4h of irradiation time. Since, the continuous flow mode of monolith photoreactor was used, the production rate of CO reached to maximum, then gradually reduced. This was probably due to gradual deactivation of catalyst supported over the monolith microchannels. The yield rates of different products with their selectivity are presented in Table 2. The yield of CO over 10 wt.% MMT/TiO_2 was 25.95 µmole g-catal.$^{-1}$ h^{-1}, a 3.04 times more than the pure TiO_2 NPs. The enhanced in photoactivity was noticeably due to mesoporous structure, higher surface area, hindered charges recombination and larger illuminated surface area in monolith microchannels. The selectivity for CO production over TiO_2 increased from 90.23 to 97.91 % in 10 wt.% MMT-

loaded TiO_2 samples. These results show that CO_2 can efficiently and continuously be converted to CO using MMT-loaded TiO_2 catalyst and monolith photoreactor.

Table 2: Summary of yield rates and selectivity of products over TiO_2 and MMT/TiO_2 samples

Samples	Yield rate μmole g-catal.$^{-1}$h^{-1}			Selectivity (%)	
	CO	CH_4	C_2H_6	CO	CH_4
TiO_2	8.52	0.92	-	90.23	9.76
10% MMT/TiO_2	25.95	0.53	0.06	97.91	2.02

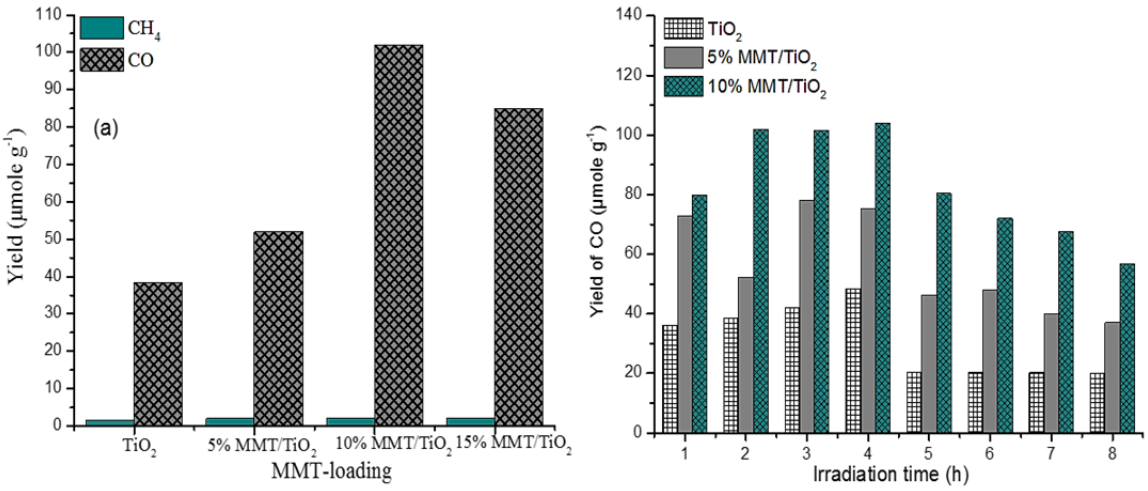

Figure 3: (a) Effect of MMT loading onto TiO_2 activity for CO_2 reduction with H_2; (b) dynamic CO evolution over TiO_2/MMT samples during RWGS reaction at 100 ^oC, CO_2/H_2 ratio 1.0 and feed flow 20 mL/min.

3.3 Reaction mechanism

During the photocatalytic reverse water gas shift reaction, CO_2 is reacted with H_2 for the production of CO and water with the smaller amounts of CH_4 and C_2H_6 as the potential products over MMT/TiO_2 samples. Therefore, possible reaction mechanism is illustrated in Eq(1)-(5).

$$TiO_2 \longrightarrow e^- + h^+ \quad (1)$$

$$MMT + e^- \longrightarrow MMT - e^- \quad (2)$$

$$CO_2 + H_2 \longrightarrow CO + H_2O \text{ (RWGSR)} \quad (3)$$

$$CO_2 + 2H_2 \longrightarrow CH_4 + O_2 \quad (4)$$

$$2CO_2 + 3H_2 \longrightarrow C_2H_6 + 2O_2 \quad (5)$$

First, electron-hole pairs were produced under light irradiation as explained in Eq(1). The photo-generated electrons can be trapped by metals in MMT, resulting in their efficient separation (Eq2). The electrons transferred toward CO_2 for its reduction while holes consumed for H_2 oxidation, resulting in RWGS reaction of CO_2 reduction (Eq 3). The, H^+ radicals and active electrons can reduce CO_2 to CH_4 and C_2H_6 as explained in Eqs (4) and (5). As discussed previously, CO was the main product with selectivity above 98%, confirming favorable RWGS reaction for CO_2 reduction to CO over MMT-loaded TiO_2 nanocomposites in a continuous operation of monolith photoreactor. The schematic presentation of CO_2 reduction via RWGS reaction is depicted in Figure 4.

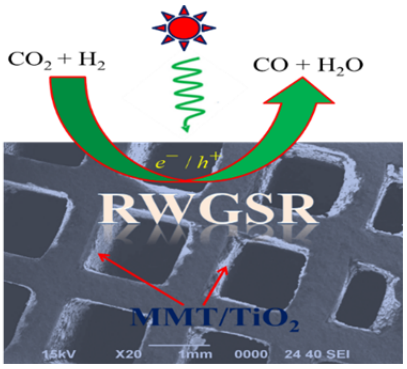

Figure 4: Schematic presentation of photocatalytic RWGS reaction inside the monolith channels.

4. Conclusions

Photocatalytic reverse water gas shift (RWGS) CO_2 reduction by H_2 for dynamic CO evolution over TiO_2 nanoparticles dispersed in MMT was investigated. CO_2 was efficiently converted to CO and hydrocarbons by introducing MMT into TiO_2 with optimum MMT-loading of 10 wt. %. The yield rate of CO as the key product observed over MMT/TiO_2 was 25.95 µmole-g-cat $^{-1}h^{-1}$ at selectivity 98%, much higher when compared with pure TiO_2 photocatalyst. Therefore, it is concluded that MMT-loaded TiO_2 is an efficient photocatalyst for RWGS CO_2 reduction to CO in a continuous operation of monolith photoreactor.

Acknowledgements

The authors would like to extend their deepest appreciation to Universiti Teknologi Malaysia for the financial support of this research under PAS-RUG (Potential Academic Staff Research University Grant, Vot 02k24).

Reference

Chen D., Zhu Q., Zhou F., Deng X., Li F., 2012, Synthesis and photocatalytic performances of the TiO2 pillared montmorillonite, Journal of hazardous materials 235-236, 186-193.

Kameshima Y., Tamura Y., Nakajima A., Okada K., 2009, Preparation and properties of TiO2/montmorillonite composites, Applied Clay Science 45 (1-2), 20-23.

Olivo A., Trevisan V., Ghedini E., Pinna F., Bianchi C.L., Naldoni A., Cruciani G., Signoretto M., 2015, CO2 photoreduction with water: Catalyst and process investigation, J. CO2 Util. 12, 86-94.

Paulino P.N., Salim V.M.M., Resende N.S., 2016, Zn-Cu promoted TiO2 photocatalyst for CO2 reduction with H2O under UV light, Appl. Catal. B: Environ. 185, 362-370.

Tahir B., Tahir M., Amin N.S., 2015a, Photoreactor Carbon Dioxide Reduction with Hydrogen in a Continuous Catalytic Monolith Photoreactor, Chem. Engin. Trans. 45, 259-264.

Tahir M., Amin N.A.S., 2013, Photocatalytic reduction of carbon dioxide with water vapors over montmorillonite modified TiO2 nanocomposites, Appl. Catal. B: Environ. 142-143, 512-522.

Tahir M., Amin N.S., 2016a, Performance analysis of nanostructured NiO–In2O3/TiO2 catalyst for CO2 photoreduction with H2 in a monolith photoreactor, Chem. Eng. J. 285, 635-649.

Tahir M., Tahir B., 2016b, Dynamic photocatalytic reduction of CO2 to CO in a honeycomb monolith reactor loaded with Cu and N doped TiO2 nanocatalysts, Appl. Surf. Sci. 377, 244-252.

Tahir M., Tahir B., Amin N.A.S., 2015b, Gold-nanoparticle-modified TiO2 nanowires for plasmon-enhanced photocatalytic CO2 reduction with H2 under visible light irradiation, Appl. Surf. Sci. 356, 1289-1299.

Tahir M., Tahir B., Amin N.A.S., 2015c, Photocatalytic CO2 reduction by CH4 over montmorillonite modified TiO2 nanocomposites in a continuous monolith photoreactor, Mater. Res. Bull. 63, 13-23.

Yang M.-Q., Xu Y.-J., 2016, Photocatalytic conversion of CO2 over graphene-based composites: current status and future perspective, Nanoscale Horiz. 1 (3), 185-200.